Proceedings of the Korean Nuclear Society Spring Meeting
Cheju, Korea, May 2001

Correlation between Zirconium Oxide Impedance and Corrosion Behavior of Zr-Nb-Sn-Fe-Cu Alloys

Sang Yoon Park, Myung Ho Lee, Byoung Kwon Choi, Yong Hwan Jeong, Youn Ho Jung
KAERI, Nuclear Fuel Cladding Team, PO Box 105, Yusong, Taejon 305-600, South Korea

Abstract

To evaluate the correlation of Zr oxide impedance and corrosion behavior of Zr-Nb-Sn-Fe-Cu alloys, the corrosion behavior of the alloys was tested in the autoclave containing 70 ppm LiOH solution at 360°C. The characteristics of the oxide on the alloys were investigated by using the electrochemical impedance spectroscopy (EIS) method. The corrosion resistance of the alloys was evaluated from the corrosion rate determined as a function of the concentration of Nb. The equivalent circuit of the oxide was composed on the base of the spectrum from EIS measurements on the oxide layers that had formed at pre- and post-transition regions on the curve of corrosion rate. By using the capacitance characteristics of the equivalent circuit, the thickness of impervious layer, it's electrical resistance and characteristics of space charge layer were evaluated. The corrosion characteristics of the Zr-Nb-Sn-Fe-Cu alloys were successfully explained by applying the EIS test results.

1. Introduction

Since pressurized water reactors (PWRs) tend to be operated in severer environments such as increased burn-up, higher operation temperature and pH, more corrosion-resistant alloys than Zircaloy-4 have been continuously developed as a substitute for Zircaloy-4[1-4]. It was known that the addition of Nb to Zircaloys would improve the corrosion resistance of Zircaloys and would reduce their hydrogen pickup during the corrosion [5,6]. Kim et al.[7] reported the manufacturing process of Zr-1Nb-0.2Cu and Zr-0.2Nb-1.3Sn-0.4Fe-0.2Cr-0.1Cu alloys and their corrosion resistance. They also reported the correlation of heat treatment to the corrosion behavior of Zn-Nb-Sn-Fe-Cu alloys[8]. But the corrosion resistance of the alloys was tested at a 400°C steam condition. In modern PWRs, lithium is added to primary coolant to maintain the recommended coolant pH between 7.1 and 7.4 [1]. So, the corrosion behavior of the new alloys in the lithiated environment is very important. Several investigations had used electrochemical impedance spectroscopy (EIS) of oxidation films on zirconium alloy to characterize internal oxide properties, that is, to allow insights into the

microstructure of the growing oxide film and more importantly to study the impervious layer at the metal-oxide interface and penetration of the electrolyte into the porous layer on the water side [9-10].
In this study, the corrosion resistance in 70 ppm LiOH solution at 360°C of Zr-Nb-Sn-Fe-Cu alloys containing 0.05 ~ 0.6% Nb was evaluated and the oxides on the alloys sampled at pre- and post-transition period were analyzed by EIS.

2. Experimental details

2.1 Sample preparation and high temperature corrosion

Many kinds of Zr-Nb-Sn-Fe-Cu alloys were produced as button-shaped 200 g ingots by vacuum arc re-melting. The chemical compositions of the alloys are shown in Table 1. b -Quenching was conducted to homogenize the composition within the ingots. The ingots were then made into the plate specimens of about 1 mm thickness through various rolling and intermediate annealing processes as shown in previous work[8]. The specimens were prepared for corrosion test after final heat treatment at 570° C for two hours.

Rectangular-shaped specimens, 15 x 25 mm^2 in size, were made through mechanical grinding with SiC paper (2400# in the final step). The out-pile corrosion test was conducted at a 360 ° C in the static autoclave filled with 70 ppm aqueous LiOH solution under the pressure of 2,750 psi. The corrosion resistance of the specimens was evaluated by measuring their weight gain per unit surface area in relation to the exposure time.

2.2 EIS measurement of the zirconium oxide

The EIS measurements were made using an impedance spectrum analyzer (Zahner IM5d), which was connected to a three-electrode electrochemical cell(EG&G PAR K0235 Flat Cell). Spectra were obtained at open-circuit potential (OCP) of the oxide electrode, with the amplitude of 10 mV. The frequency span was normally from 0.5 mHz to 1 MHz. The working electrode was the Zr oxide corroded in 360° C LiOH solution for 60 and 300 days. The auxiliary electrode was the platinum grid. A saturated calomel electrode (SCE) connected to the cell by a bridge with a Luggin capillary served as a reference electrode. All potentials quoted in the paper are referred to those from the electrode. Before EIS measurement, the oxide was soaked in test solution as an electrode for 20 hours, and the electrode potential was monitored. The solution was 0.05M H_2SO_4 prepared from analytical grade materials (Junsei) and deionized water by ultra pure water system (Nanopure MD4744).

3. Results and discussion

3.1 Corrosion behavior of Zr-Nb-Sn-Fe-Cu alloys

Fig.1 shows the corrosion behavior of some alloys in Zr-0.2Nb-1.1Sn-Fe-Cu alloy system with changing Nb content from 0.05wt.% to 0.3wt.%, respectively. It is found in the Fig.1 that the corrosion behavior of the alloys compares to that of a commercial low Sn Zircaloy-4(Zry-4), which is being used for commercial PWRs.

All the alloys showed very similar corrosion behaviors for 150 days without any remarkable effect in spite of the different Nb content in the alloys while the corrosion rate of them showed the transition after 150 days with increasing the corrosion resistance of them as the addition of Nb to the alloys became larger in amount. Especially, the second transition of the rate occurred after 270 days and the slope of the graph in the Fig.1 indicates that the rate of corrosion would be faster after the second transition if Nb content became less in the alloys.

The corrosion rate of the Zry-4 showed the transition after 60 days and was significantly accelerated after 180 days. In other word, the Zr-0.2Nb-1.1Sn-Fe-Cu alloys had more outstanding corrosion resistance than that of the Zry-4 in LiOH solution.

Fig. 2 indicates the effect of addition of Nb to both Zr-0.2Nb-1.1Sn-Fe-Cu and Zr-0.4Nb-0.8Sn-Fe-Cu alloy systems after 300 days in the corrosion test. In those alloy systems, the addition of only Nb to the alloys have changed from 0.05wt.% to 0.3wt.% and from 0.3% to 0.6wt.%, respectively while Sn content was fixed at 1.1wt.% and 0.8wt.%. As Nb content became larger in the alloy specimens, the corrosion resistance of the specimens increased with the decrease of weight gain. The result was consistent with the report that the Zr-based alloys showed good corrosion resistance bearing no relation to any effect of the annealing parameter when the Nb added to the alloys within its solubility limit [4].

The weight gain of the specimens in the test tends to be changed in relation to Nb content in the alloys as showed in Fig.2. It can be expressed as follows.

$$WG_{1.1Sn} = - 16.51 \ln[Nb] + 77.11 \quad \text{..... (1)}$$

$$WG_{0.8Sn} = - 11.05 \ln[Nb] + 74.00 \quad \text{..... (2)}$$

If Nb content were fixed in the above alloy systems, the weight gain of the alloys can be easily calculated according to the equation (1) and (2). It can be also found that the effect of weight gain due to the increase of Nb content in 1.1wt.% Sn alloy system is bigger than that in 0.8wt.% Sn alloy system.

3.2 EIS Characteristics of Zr Oxides

Fig. 3 shows the open circuit potentials (OCPs) depending on the test time of the oxide on the Zr-based alloys. It was drawn from the measurement of OCPs of the electrode, which were soaked as the oxide in an electrolyte, in order that the electrolyte can contact enough the voids in or on the oxide before measuring electrochemical impedance spectroscopy (EIS) in 0.05M sulfuric-acid liquid solution. The tested oxide was that formed on the alloy, which contain 0.4wt.% Nb and 0.8wt.% Sn when it has corroded for 60 days before and for 300 days after transition of the corrosion rate.

The OCPs did not show many differences from each other in early test but they showed many differences between them later on. After about 200 minutes from the start of the test, the voltage differences showed over 1.3 between the COPs from the oxide before its transition of corrosion rate and the COPs from the one after the transition. From this result it was supposed that ZrO_{2-x}, which showed good passivity, formed during the early corrosion process and transformed into the unstable ZrO_2 that take the longer test time to be formed. It appeared that the electric potential of the electrode have increased as long as the oxidation of the alloy kept. There was an outstanding increase in the amplitude of the electrode potential within 200 minutes after the transition of corrosion rate. It was inferred from the test results that the electrical potential have increased because the electrolyte had contacted the pores in the ZrO_2 oxide that have high oxidation value due to penetrating the electrolyte into a lot of pores on the oxide formed after the transition of the corrosion rate. Therefore, it is possible to predict the degree of pores on the oxide through measuring the changes of OCPs from the oxide.

Fig. 4 shows the impedance spectra of the oxide depending on the change of frequency before and after the transition of corrosion rate of Zr-based 0.2Nb1.1Sn alloy system. The slope of oxide impedance to frequency was -0.94 (nearly -1) before the transition for all the range. The phase of the oxide before the transition was close to 90° for the large frequency range. Accordingly, it is possible that the whole oxide has good corrosion resistance since it has good capacitance characteristics and the spacer-charge layer on its surface.

However, the oxide after the transition has very different characteristics from the one before transition. In case of high frequency, The slope of impedance to frequency was - 0.91, which was similar to that of the oxide before transition for all the range, but with going down to low frequency range the value of impedance was getting lowered, and the slope was -0.63 and the phase value became also lowered showing two peaks. Therefore, it was understood that two layers on the oxide were found to have different characteristics because there was different impedance characteristics between the high and the low frequency range.

Fig. 5 draws the oxide model having two film layers and the equivalent circuit to explain the impedance spectrum, which is applicable to the analysis of corrosion phenomenon of the alloys. It is known that the model is fit for explaining the formation of TiO_2 or Al_2O_3 oxides [11-13].

A corrosion test on the Zircaloy-4 alloy was performed in 70 ppm LiOH solution at 360 to investigate its oxide properties [14]. It was reported as the results of the test that Li element existed in the voids or incorporated into ZrO_2 network because the oxide have the protective film at its inner layer before acceleration of the corrosion and it has porous non-protective film at its outer layer. It was also reported that the protective inner layer was getting very thin or vanished away while Li element deeply permeated into the oxide. Accordingly, the above model could be effectively used to interpret the impedance spectrum of the ZrO_2 oxides.

From the comparison of the impedance spectrum from the test with the equivalent circuit in the Fig. 8, it is possible to calculate the capacitance and resistance of the inner and outer layers on the oxide that had been formed at each corrosion condition. In particular, the thickness of inner layer indicating the corrosion resistance can be calculated from the capacitance value of the layer on the oxide. There is the following relationship between the impedance and the thickness from ideal flat capacitor [10].

$$Z = \frac{t}{2pfeeoA} \quad \text{---------- (3)}$$

Where, f = frequency

A = surface area

å = absolute dielectric constant, 8.86 x 10^{-12} F/m

$å_o$ = relative dielectric constant of ZrO_2

Since the impedance is noted as $Z = 1/2pfC$ in case of the capacitance, the thickness of the capacitance expresses as follows.

$$t = \frac{eeoA}{C} \quad \text{---------- (4)}$$

Where, the unit of *t* is nm, the unit of *C* is ì F/cm^2.

Because there is a reciprocally proportional relationship between the capacitance and the thickness of the oxide film, the thickness can be calculated if the value of the capacitance for the non-permeated oxide film obtained by the analysis of the components of EIS spectrum and equivalent circuit.

The value of $å_oå$ for ZrO_2 in the equation (4) is used from 13 to 22[8]. If the value could be measured exactly for the inner and porous outer of the oxide, it would be easy to expect the thickness of oxide film and the corrosion resistance of the alloy specimens in the autoclave. The values calculated for the characteristics

of oxide film were listed in the table 2, where the subscript "P" stands for porous film on the outer side of oxide and the subscript "B" stands for non-permeated film on the inner side of oxide. The values of Tt are the thickness between the inner and the outer layer of the oxide calculated from the equation, and those of Tm are the whole thickness of the oxide calculated from the weight gain of the specimen.

The thickness of oxide before the transition of the corrosion rate was relatively well agreed within the acceptable test-error limits with the one measured using the weight gain as well as the one calculated using the EIS method. However, The equation (4) was not applicable to estimate the thickness of the porous oxide film since the thickness of oxide after the transition was out of the acceptable error limit because it had high difference on the oxide.

3.3 Electrical resistance of Zr oxides

Fig. 6 shows the electrical resistance characteristics of the duplicate oxides calculated from the analysis of the EIS spectrum, which had got from the tests. It is found from the Fig.6 (a) that the electrical resistance of the outer oxide film had remarkably decreased after the transition while that of the inner oxide film had reduced by a half of its original one. But as shown in the Fig.6 (b), the thickness of the inner and the outer oxide film increased 3 times as much as that before the transition, and the ratio of the thickness of the inner and the outer was 45:55 with having the outer a little thicker. The resistance value of the inner and the outer divided by the oxide thickness was shown in the Fig.6(c) to compare the specific resistance of the oxide.

It was found from the above result that the resistance value of the outer oxide decreased by about 1/100 while that of the inner became less by 1/7, the electrical characteristics of the outer oxide got badly worse. So, it is understood that the cracks or pores are formed on the outer layer of the oxide and electrolyte permeates into them as well as the model about the equivalent circuit and oxide film is quite reasonable.

In summary, it seems that the corrosion rate of the alloys tends to increase because the outer layer on the oxides never contributes to the corrosion resistance of the alloys and the inner layer also does not cut off effectively the transfer of electrons and oxygen ions due to the reduction of its electrical resistance.

Fig. 7 shows the specific values of electric resistance of oxides on the 0.4Nb and the 0.2Nb alloy systems after the transition. The resistance ratio for 0.4Nb to 0.2Nb of the inner layers was 10 to 8 indicating that 0.4Nb alloy system was more resistant, and the ratio of the outer layers was 20 to 1 showing that 0.2Nb alloy system has very poor resistance characteristics. However, there was a proportional relationship between the electrical resistance and the corrosion rate of the inner oxides since in the corrosion test the weight gain of 0.4Nb0.8SnFeCu alloy was 80% of that of 0.2Nb1.1SnFeCu alloy as shown in Fig.1.

4. Conclusion

The followings were concluded from the investigation of the EIS characteristics of the oxides on both Zr-0.2Nb-1.1Sn-Fe-Cu and Zr-0.4Nb-0.8Sn-Fe-Cu alloy systems, and the corrosion test of those alloy systems to study their corrosion characteristics in the autoclave at high temperature and pressure.

(1) The more the alloys had Nb content the more the corrosion resistance tended to increase within 0.05wt.% to 0.6wt.% and the weight gain of the alloys decreased logarithmically as the Nb content increased. The more the alloys had Sn content the more the corrosion resistance tended to decrease and the weight gain increased in proportion to the Sn content. Using the curve-fitting method the equations were derived as follows for the relationship of weight gain to the Nb and Sn content.

$WG_{1.1Sn} = -16.51 \ln[Nb] + 77.11$

$WG_{0.8Sn} = -11.05 \ln[Nb] + 74.00$

(2) The thickness of oxides calculated from capacitance values was in well agreement with that calculated from the measurement of weight gain when the characteristics of the oxides with the duplicate structure was evaluated by analyzing the absolute values of impedance and the phases of the oxides.

(3) The electrical resistance of the inner layer on the oxides after the transition of corrosion rate decreased by 1/7 and that of the outer layer by 1/100 comparing to that before the transition when calculated the electrical resistance of the inner and outer layer on the oxides from the EIS measurement data. There was a close relationship between the electrical resistance of the inner oxide and the characteristics of long term corrosion of the alloys.

Acknowledgement

This project has been carried out as a part of the nuclear R&D program by MOST.

References

1. S. Anthoni, P. Ridoux, O. Menet and C. Weber, "Water Chemistry of Nuclear Reactor Systems," British Nuclear Energy Society (BNES), Bournemouth, UK, 1992, p. 9.
2. F. Garzarolli, H. Stehle, E. Steinberg, in: Zirconium in the Nuclear Industry, ASTM STP 1295 (1996) 12.
3. G.P. Sabol and S.G. McDonald : Nucl. Sci. & Eng. 63, 1977, p. 83.
4. T. Isobe, T. Matsuo, Y. Mae, in: Zirconium in the Nuclear Industry, ASTM STP 1245 (1994) 437.
5. G.P. Sabol, R.J. Comstock, R.A. Weiner, P. Larouere, R.N. Stanutz, in: Zirconium in the Nuclear Industry, ASTM STP 1245 (1994) 724.
6. A.V. Nikulina, V.A. Markelov, M.M. Peregud, Y.K. Bibilashvili, V.A Kotrekhov, A.F. Losistsky, N.V.

Kuzmeko, Y.P. Shevnin, V.K. Shamardin, G.P. Nobylyansky, A.E. Novoselov, in: Zirconium in the Nuclear Industry, ASTM STP 1295 (1996) 785

7. J.M. Kim, Y.H. Jeong, Y.H. Jung, Metals and Materials, 6, 2, 2000, p 139.
8. J.M. Kim, Y.H. Jeong, Y.H. Jung, J. Materials Processing Tech., 104, 2000, p 145.
9. B. Cox and C. Wu, J. Nucl. Mater., 224, 1991, p. 169.
10. P. Barberis and A. Frichet, J. Nucl. Mater., 273, 1999, p. 182.
11. J. Pan, D. Thierry and C. Leygraf, Electrochemica Acta, 41, 1996, p. 1143.
12. F. Mansfeld, Analysis and Interpretation of EIS Data for Metals and Alloys, Chapter 4, Technical Report 26, Solartron-Schlumberger.
13. A. Baltat - Baaia, N. Celati, M. Keddam, H. Takenouti and R. Wiart, Mater. Sci. Forum, 111, 1992, p. 359
14. P. Dominique, G. Jeol, B. Philippe and T. Jeol, in: Zirconium in the Nuclear Industry, ASTM STP 1295 (1996) 94.

Table 1. Chemical composition of the test alloys

Alloy Group	Chemical Composition			
	Nb	Sn	Fe	Cu
Zr-0.2Nb-1.1Sn-*x*Fe-*y*Cu	0.05	1.1	*x*	*y*
	0.1	1.1	*x*	*y*
	0.2	1.1	*x*	*y*
	0.3	1.1	*x*	*y*
	0.2	0.9	*x*	*y*
	0.2	1.3	*x*	*y*
Zr-0.4Nb-0.8Sn-*x*Fe-*y*Cu	0.3	0.8	*x*	*y*
	0.4	0.8	*x*	*y*
	0.5	0.8	*x*	*y*
	0.6	0.8	*x*	*y*
	0.4	0.7	*x*	*y*
	0.4	0.8	*x*	*y*

Table 2. Electrochemical properties of the oxide layer

Oxide Group	Items	Value	1/C	Tt(μm)[1)]	Tm(μm)[2)]
Pre-Transition oxide (Zr-o.2Nb-1.1Sn-xFe-yCu)	R_E(Ω)	49.1	-	-	-
	R_P(M Ω)	234.3	-	-	-
	C_P(nF)	15.5	1.2	2.1	2.07
	C_B(nF)	20.4	0.9		
	R_B(G Ω)	1.2	-		
Post-Transition oxide (Zr-0.2Nb-1.1Sn-xFe-yCu)	R_E(Ω)	40.0	-	-	-
	R_P(M Ω)	7.9	-	-	-
	C_P(nF)	6.2	3.1	3.2	6.88
	C_B(nF)	138.0	0.1		
	R_B(G Ω)	0.6			
Post-Transition oxide (Zr-0.4Nb-0.8Sn-xFe-yCu)	R_E(Ω)	42.2	-	-	-
	R_P(M Ω)	112.0	-	-	-
	C_P(nF)	6.1	3.1	3.4	5.70
	C_B(nF)	53.0	0.3		
	R_B(G Ω)	0.8	-	-	-

1) $T_c = 1/C_P + 1/C_B$ (= Calculated Total Thickness)

2) Tm = Measured Total Thickness by Weight Gain($1\mu m = 15 mg/dm^2$)

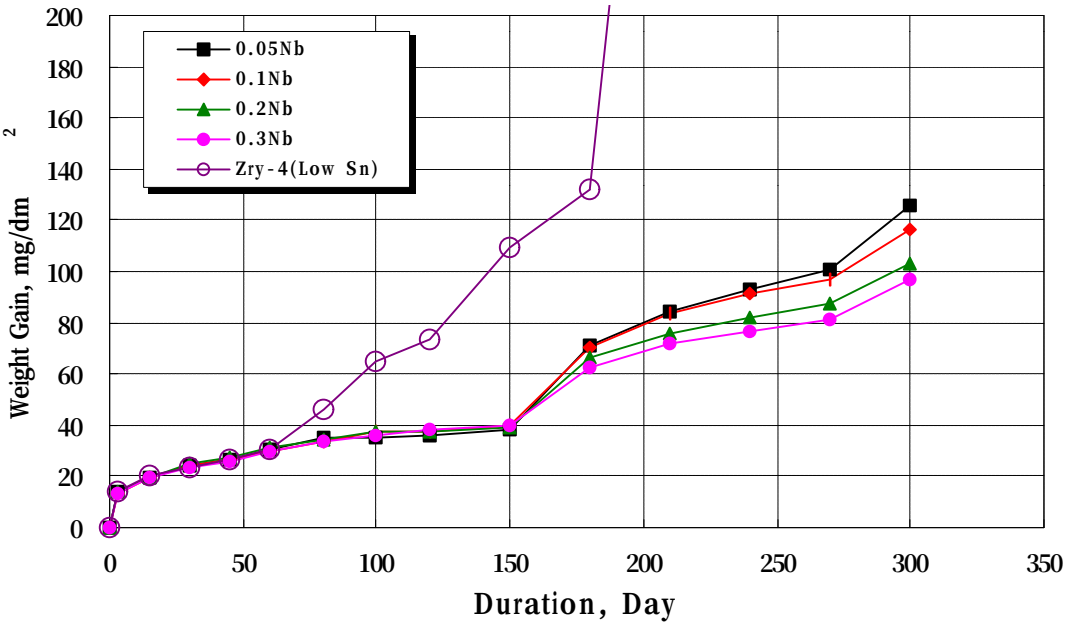

Fig. 1. Corrosion behavior of the Zr-0.2Nb-1.1Sn-Fe-Cu alloys with different Nb content in 70 ppm LiOH solution.

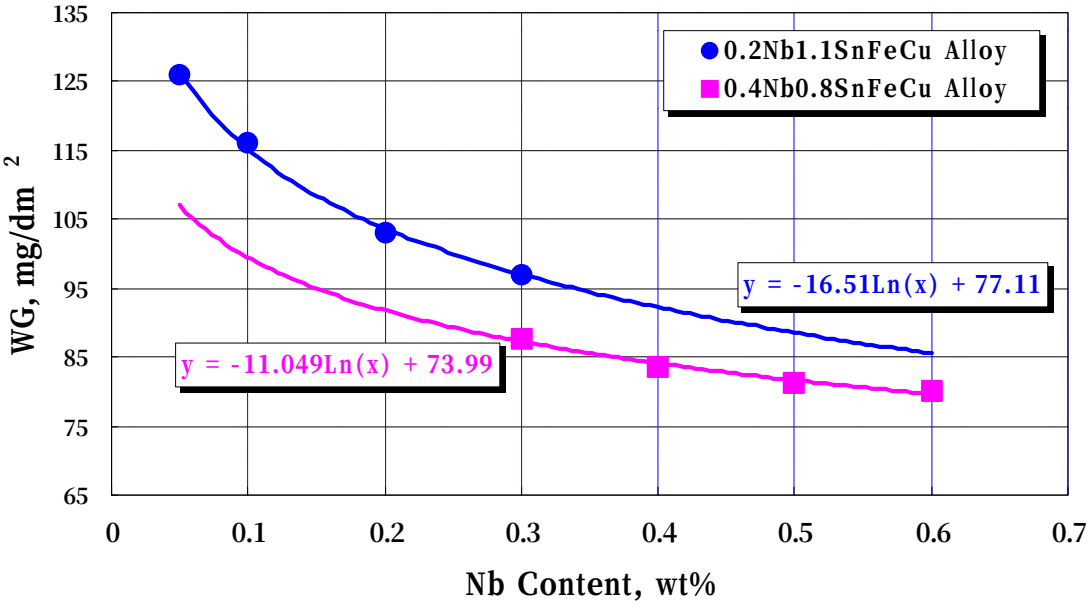

Fig. 2. Effect of Nb content on the corrosion of Nb containing Zr alloys.

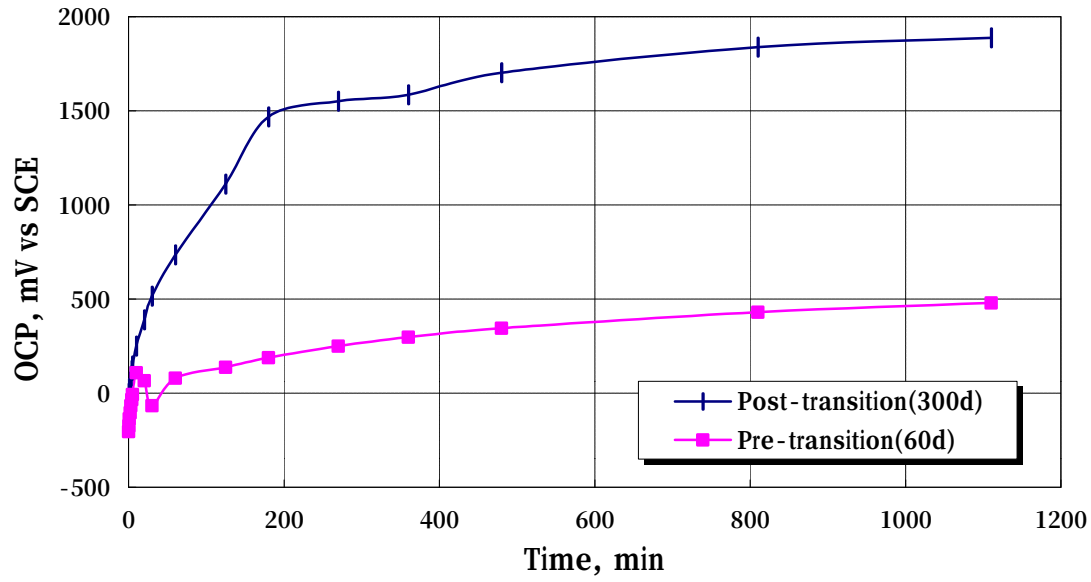

Fig. 3. Open Circuit Potentials vs. time of the Zr oxide layers.

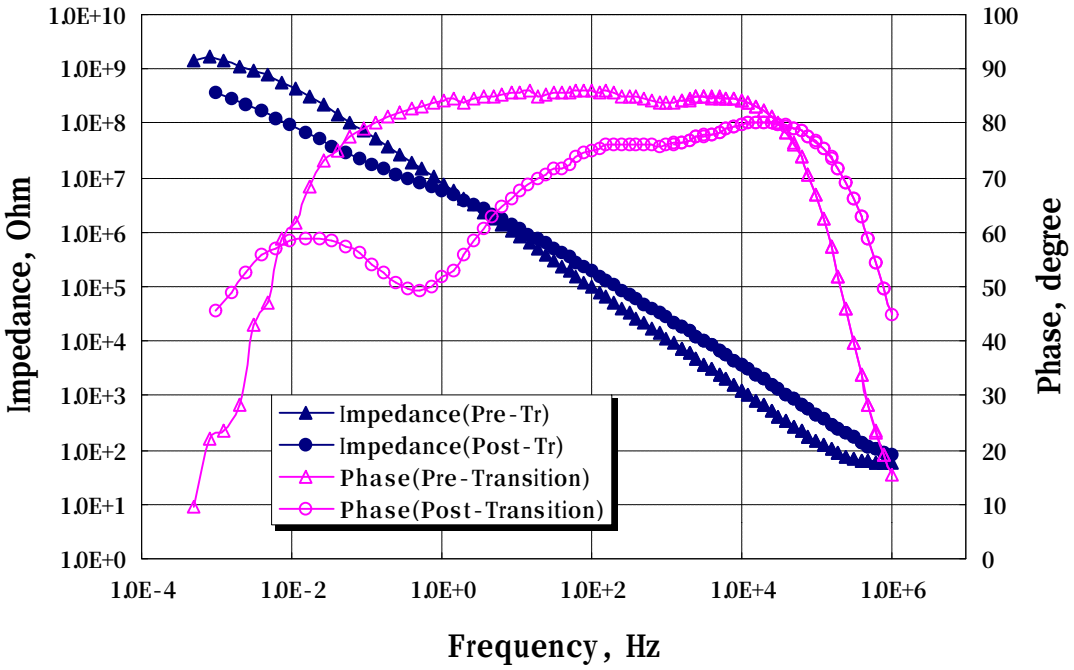

Fig. 4. Comparison of the impedance spectra between pre- and post-transition oxide of the 0.2Nb1.1Sn-Fe-Cu alloy.

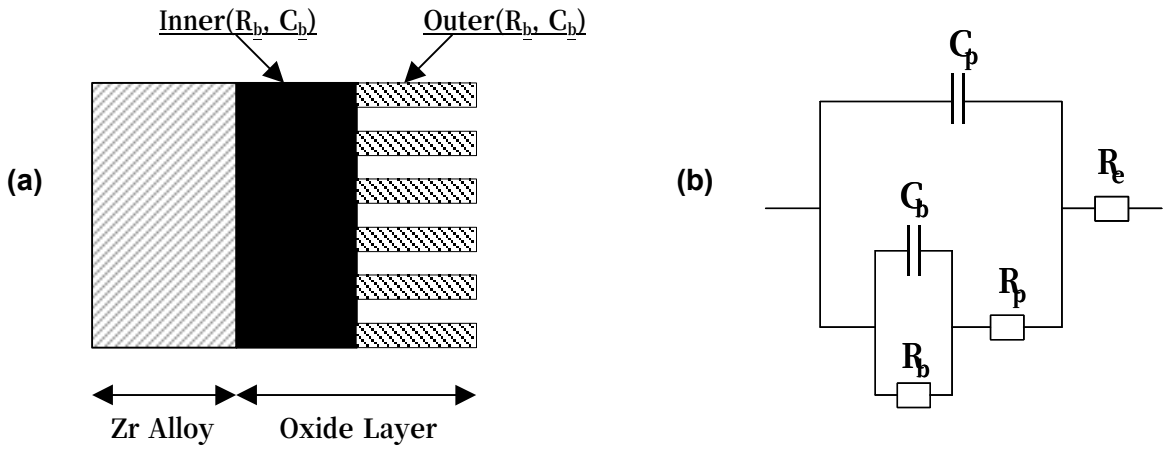

Fig. 5. Schematic representation for the oxide layer formed on the Zr alloy surface (a) and it' s equivalent circuit. Notations (b) : Re is the solution resistance; Cb and Rb are the inner layer capacitance and resistance; Cp and Rp are the outer layer capacitance and resistance.

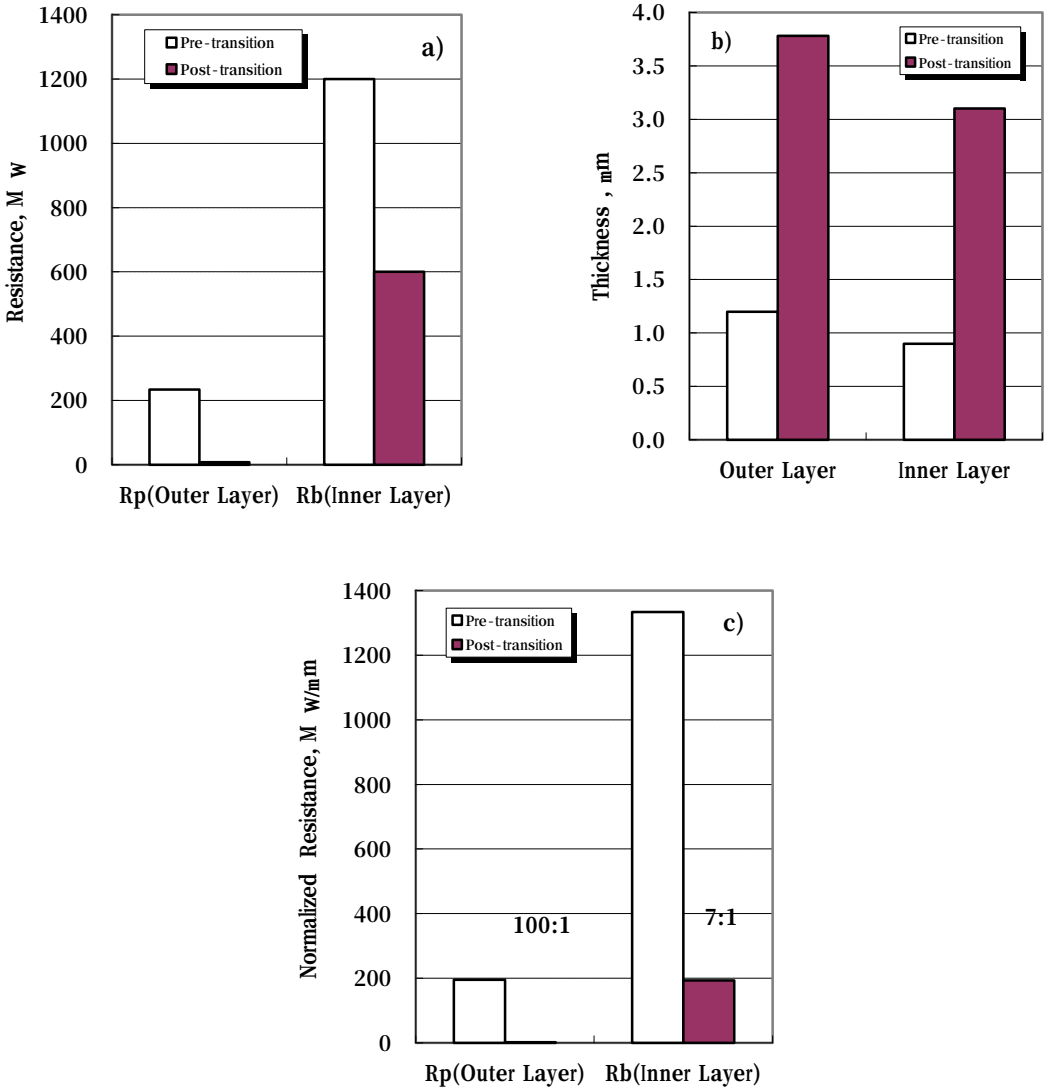

Fig. 6. Comparison of the electric resistance(a), oxide thickness(b) and normalized electric resistance(c) between inner and outer oxide layer.

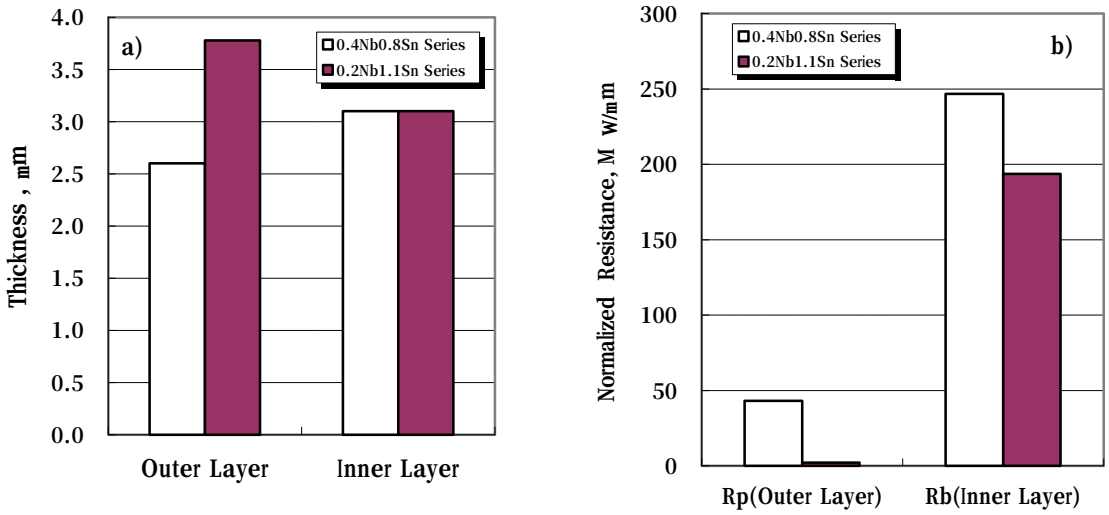

Fig. 7. Comparison of the oxide thickness(a), normalized electric resistance(b) between inner and outer oxide layer.